

submitted to *The Astrophysical Journal*

## On Radiation Pressure in Static, Dusty H II Regions

B.T. Draine

*Princeton University Observatory, Peyton Hall, Princeton, NJ 08544;*  
 draine@astro.princeton.edu

### ABSTRACT

Radiation pressure acting on gas and dust causes H II regions to have central densities that are lower than the density near the ionized boundary. H II regions in static equilibrium comprise a family of similarity solutions, parametrized by 3 parameters:  $\beta$ ,  $\gamma$ , and the product  $Q_0 n_{\text{rms}}$ ;  $\beta$  characterizes the stellar spectrum,  $\gamma$  characterizes the dust/gas ratio,  $Q_0$  is the ionizing output from the star (photons/s), and  $n_{\text{rms}}$  is the rms density within the ionized region. Adopting standard values for  $\beta$  and  $\gamma$ , varying  $Q_0 n_{\text{rms}}$  generates a one-parameter family of density profiles, ranging from nearly uniform density H II regions for small  $Q_0 n_{\text{rms}}$ , to hollow-sphere H II regions for large  $Q_0 n_{\text{rms}}$ . When  $Q_0 n_{\text{rms}} \gtrsim 10^{52} \text{ cm}^{-3} \text{ s}^{-1}$ , dusty H II regions have conspicuous central cavities, even if no stellar wind is present. For given  $\beta$ ,  $\gamma$  and  $Q_0 n_{\text{rms}}$ , a fourth quantity, which can be taken to be  $Q_0$ , determines the overall size and density of the H II region. Examples of density and emissivity profiles are given, and we show how quantities of interest such as the peak-to-center emissivity ratio, the edge-to-rms density ratio, and the fraction of the ionizing photons absorbed by the gas depend on the 3 parameters  $\beta$ ,  $\gamma$ , and  $Q_0 n_{\text{rms}}$ . For dusty H II regions, compression of the gas and dust into an ionized shell results in a substantial increase in the fraction of the  $h\nu > 13.6 \text{ eV}$  photons that actually ionize H. We discuss how radial drift of dust grains in H II regions can alter the dust-to-gas ratio. The applicability of these solutions to real, non-static H II regions is discussed.

*Subject headings:* ISM: bubbles; dust, extinction; HII regions; ISM: structure; infrared: ISM; radio continuum: ISM

### 1. Introduction

Strömgren (1939) idealized photoionized nebulae around hot stars as static, spherical regions with a uniform density of ionized gas out to a bounding radius  $R$ . The Strömgren sphere model continues to serve as the starting point for studies of H II regions around hot stars. However, a number of physical effects lead to departures from the simple Strömgren sphere model: dynamical expansion of the H II region if the pressure in the surrounding neutral medium cannot confine the

ionized gas; deviations from sphericity due to nonuniform density; motion of the star relative to the gas; injection of energy and momentum by a stellar wind; absorption of H-ionizing photons by dust grains; and radiation pressure acting on gas and dust. Each of these effects has been the object of a number of investigations, beginning with the study of ionization fronts by Kahn (1954).

Savedoff & Greene (1955) appear to have been the first to discuss the expansion of a spherical H II region in an initially uniform neutral medium. Mathews (1967, 1969) and Gail & Sedlmayr (1979) calculated the dynamical expansion of an H II region produced by an O star in a medium that was initially neutral, including the effects of radiation pressure acting on the dust. Mathews (1967, 1969) showed that radiation pressure on dust would produce low-density central cavities in H II regions. More recently, Krumholz & Matzner (2009) reexamined the role of radiation pressure on the expansion dynamics of H II regions, concluding that radiation pressure is generally unimportant for H II regions ionized by a small number of stars, but is important for giant H II regions surrounding clusters containing many O-type stars. Their study concentrated on the forces acting on the dense shell of neutral gas and dust bounding the H II region, hence they did not consider the density structure within the ionized region.

In addition to acting as an agent for radiation pressure, dust absorbs  $h\nu > 13.6\text{eV}$  photons that would otherwise be able to ionize hydrogen, thereby reducing the extent of the ionized zone. Petrosian et al. (1972) developed analytic approximations for dusty H II regions. They assumed the gas density to be uniform, with a constant dust-to-gas ratio, and found that dust could absorb a substantial fraction of the ionizing photons in dense H II regions. Petrosian et al. gave attention to the ionization structure, but did not consider the effects of radiation pressure. Somewhat suprisingly, the simple problem of static equilibrium H II regions with radiation pressure and dust both included does not appear to have been analyzed.

The present paper discusses the structure of dusty H II regions that are assumed to be in equilibrium with an external bounding pressure. The assumptions and governing equations are presented in §2, where it is shown that dusty H II regions are described by a 3-parameter family of similarity solutions. In §3 we show density profiles for selected cases, as well as surface brightness profiles. The fraction of the ionizing photons absorbed by dust is calculated. Dust grain drift is examined in §4, where it is shown that it can alter the dust-to-gas ratio in high density H II regions. The results are discussed in §5, and summarized in §6.

## 2. Equilibrium Model

Consider the idealized problem of a static, spherically-symmetric equilibrium H II region ionized by a point source, representing either a single star or a compact stellar cluster. Assume a constant dust-to-gas ratio (the validity of this assumption will be examined later). For simplicity, ignore scattering, and assume  $\sigma_d$ , the dust absorption cross section per H nucleon, to be independent of photon energy  $h\nu$  over the  $\sim 5\text{eV}$  to  $\sim 30\text{eV}$  range containing most of the stellar power.

Let the star have luminosity  $L = L_n + L_i = L_{39} 10^{39} \text{ ergs s}^{-1}$ , where  $L_n$  and  $L_i$  are the luminosities in  $h\nu < 13.6 \text{ eV}$  and  $h\nu > 13.6 \text{ eV}$  photons, respectively. The rate of emission of  $h\nu > 13.6 \text{ eV}$  photons is  $Q_0 \equiv 10^{49} Q_{0,49} \text{ s}^{-1}$  and the mean energy of the ionizing photons is  $\langle h\nu \rangle_i \equiv L_i / Q_0$ . A single main sequence star of spectral type O6V has  $L_{39} = 0.80$  and  $Q_{0,49} = 0.98$  (Martins et al. 2005). A compact cluster of OB stars might be treated as a point source with much larger values of  $Q_{0,49}$  and  $L_{39}$ .

Ignore He, and assume the H to be nearly fully ionized, with photoionization balancing “Case B” radiative recombination, with “on-the-spot” absorption of  $h\nu > 13.6 \text{ eV}$  recombination radiation. Take the effective radiative recombination coefficient to be  $\alpha_B \approx 2.56 \times 10^{-13} T_4^{-0.83} \text{ cm}^3 \text{ s}^{-1}$  for  $0.3 \lesssim T_4 \lesssim 3$ , with  $T_4 \equiv T / 10^4 \text{ K}$ , where  $T$  is the gas temperature.

Assume the gas to be in dynamical equilibrium (the neutral gas outside the ionized zone is assumed to provide a confining pressure). Static equilibrium then requires that the force per unit volume from radiation pressure be balanced by the pressure gradient:

$$n\sigma_d \frac{[L_n e^{-\tau} + L_i \phi(r)]}{4\pi r^2 c} + \alpha_B n^2 \frac{\langle h\nu \rangle_i}{c} - \frac{d}{dr} (2nkT) = 0 \quad , \quad (1)$$

where  $n(r)$  is the proton density,  $L_i \phi(r)$  is the power in  $h\nu > 13.6 \text{ eV}$  photons crossing a sphere of radius  $r$ , and  $\tau(r)$  is the dust absorption optical depth. Eq. (1) underestimates the radiation pressure force, because it assumes that recombination radiation (including Lyman- $\alpha$ ) and cooling radiation escape freely.

The functions  $\phi(r)$  and  $\tau(r)$  are determined by

$$\frac{d\phi}{dr} = -\frac{1}{Q_0} \alpha_B n^2 4\pi r^2 - n\sigma_d \phi \quad , \quad (2)$$

$$\frac{d\tau}{dr} = n\sigma_d \quad , \quad (3)$$

with boundary conditions  $\phi(0) = 1$  and  $\tau(0) = 0$ . Define a characteristic density and length scale

$$n_0 \equiv \frac{4\pi\alpha_B}{Q_0} \left( \frac{2ckT}{\alpha_B \langle h\nu \rangle_i} \right)^3 = 4.54 \times 10^5 \frac{T_4^{4.66}}{Q_{0,49}} \left( \frac{18 \text{ eV}}{\langle h\nu \rangle_i} \right)^3 \text{ cm}^{-3} \quad , \quad (4)$$

$$\lambda_0 \equiv \frac{Q_0}{4\pi\alpha_B} \left( \frac{\alpha_B \langle h\nu \rangle_i}{2ckT} \right)^2 = 2.47 \times 10^{16} \frac{Q_{0,49}}{T_4^{2.83}} \left( \frac{\langle h\nu \rangle_i}{18 \text{ eV}} \right)^2 \text{ cm} \quad , \quad (5)$$

and the dimensionless parameters

$$\beta \equiv \frac{L_n}{L_i} = \frac{L}{L_i} - 1 = 3.47 \frac{L_{39}}{Q_{0,49}} \left( \frac{18 \text{ eV}}{\langle h\nu \rangle_i} \right) - 1 \quad , \quad (6)$$

$$\gamma \equiv \left( \frac{2ckT}{\alpha_B \langle h\nu \rangle_i} \right) \sigma_d = 11.2 T_4^{1.83} \left( \frac{18 \text{ eV}}{\langle h\nu \rangle_i} \right) \left( \frac{\sigma_d}{10^{-21} \text{ cm}^2} \right) \quad . \quad (7)$$

The parameter  $\beta$ , the ratio of the power in non-ionizing photons to the power in photons with  $h\nu > 13.6 \text{ eV}$ , depends solely on the stellar spectrum. We take  $\beta = 3$  as our standard

value, corresponding to the spectrum of a  $T_\star = 32000$  K blackbody, but we also consider  $\beta = 2$  ( $T_\star = 45000$  K) and  $\beta = 5$  ( $T_\star = 28000$  K); the latter value could apply to a cluster of O and B stars.

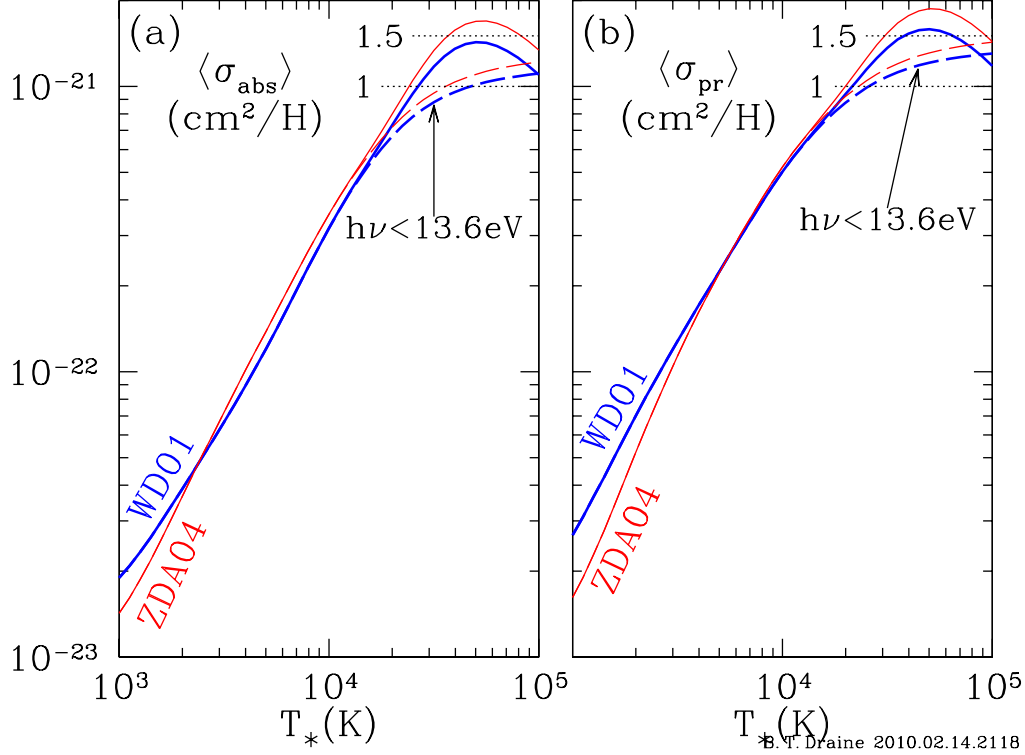


Fig. 1.— (a) Absorption cross section per H, and (b) radiation pressure cross section per H, averaged over blackbody spectra, as functions of the blackbody temperature  $T_\star$ , for the dust models of Weingartner & Draine (2001, WD01) and Zubko et al. (2004, ZDA04). Broken lines show averages over  $h\nu < 13.6$  eV only, appropriate for dust in neutral gas.

Momentum can be transferred to a dust grain by photon absorption, but also by scattering. The cross section  $\sigma_d$  appearing in eq. (1) should be  $\langle \sigma_{\text{pr}} \rangle$ , the radiation pressure cross section per H  $\sigma_{\text{pr}}(\nu) \equiv \sigma_{\text{abs}} + (1 - \langle \cos \theta \rangle) \sigma_{\text{sca}}$  averaged over the spectrum of the radiation field at radius  $r$ , where  $\sigma_{\text{abs}}(\nu)$  and  $\sigma_{\text{sca}}(\nu)$  are the absorption and scattering cross section per H, and  $\langle \cos \theta \rangle$  is the mean value of the cosine of the scattering angle  $\theta$  for photons of frequency  $\nu$ .

In eqs. (2) and (3),  $\sigma_d$  characterizes the effectiveness of the dust in attenuating the radiation field. While scattering does not destroy the photon, it does increase the probability of the photon undergoing subsequent absorption. Thus, the value of  $\sigma_d$  in eqs. (2) and (3) should exceed  $\langle \sigma_{\text{abs}} \rangle$ .

Figure 1(a) shows the dust absorption cross section per H nucleon averaged over a blackbody spectrum, for two dust models (Weingartner & Draine 2001; Zubko et al. 2004) that reproduce the wavelength-dependent extinction in the diffuse interstellar medium using mixtures of PAHs,

graphite, and amorphous silicate grains. Fig. 1(b) shows that  $\langle\sigma_{\text{pr}}\rangle$ , the radiation pressure cross section averaged over blackbody spectra, is only slightly larger than  $\langle\sigma_{\text{abs}}\rangle$ . Given the uncertainties in the nature of the dust in H II regions, it is reasonable to ignore the distinction between  $\langle\sigma_{\text{pr}}\rangle$  and the attenuation cross section and simply take  $\sigma_d = \langle\sigma_{\text{pr}}\rangle$  in eq. (1–3).

For dust characteristic of the diffuse ISM, one could take  $\langle\sigma_{\text{pr}}\rangle \approx 1.5 \times 10^{-21} \text{ cm}^2 \text{ H}^{-1}$  for  $2.5 \times 10^4 \text{ K} \lesssim T_{\text{rad}} \lesssim 5 \times 10^4 \text{ K}$ . However, dust within an H II region may differ from interstellar dust. For example, the small-size end of the size distribution might be suppressed, in which case  $\sigma_d$  would be reduced. Low metallicity galaxies will also have lower values of  $\sigma_d$ , simply because there is less material out of which to form grains. In the present work we will assume a factor  $\sim 1.5$  reduction in  $\sigma_d$  relative to the local diffuse ISM, taking  $\sigma_d \approx 1 \times 10^{-21} \text{ cm}^2 \text{ H}^{-1}$  as the nominal value, but larger and smaller values of  $\sigma_d$  will also be considered.

The dimensionless parameter  $\gamma$  depends also on the gas temperature  $T$  and on the mean ionizing photon energy  $\langle h\nu \rangle_i$ , but these are not likely to vary much for H II regions around OB stars. We take  $\gamma = 10$  as a standard value, but will also consider  $\gamma = 5$  and  $\gamma = 20$ . Low-metallicity systems would be characterized by small values of  $\gamma$ .

Switching to dimensionless variables  $y \equiv r/\lambda_0$ ,  $u \equiv n_0/n$ , the governing equations (1–3) become

$$\frac{du}{dy} = -1 - \gamma (\beta e^{-\tau} + \phi) \frac{u}{y^2} \quad , \quad (8)$$

$$\frac{d\phi}{dy} = -\frac{y^2}{u^2} - \gamma \frac{\phi}{u} \quad , \quad (9)$$

$$\frac{d\tau}{dy} = \frac{\gamma}{u} \quad , \quad (10)$$

with initial conditions  $\phi(0) = 1$  and  $\tau(0) = 0$ . The solutions are defined for  $0 < y \leq y_{\text{max}}$ , where  $y_{\text{max}}$  is determined by the boundary condition  $\phi(y_{\text{max}}) = 0$ . For each solution  $u(y)$  the root-mean-square density is

$$n_{\text{rms}} \equiv n_0 \left[ \frac{3}{y_{\text{max}}^3} \int_0^{y_{\text{max}}} \frac{y^2}{u^2} dy \right]^{1/2} \quad . \quad (11)$$

Let

$$R_{s0} \equiv \left( \frac{3Q_0}{4\pi n_{\text{rms}}^2 \alpha_B} \right)^{1/3} = 2.10 \times 10^{18} \frac{Q_{0,49}^{1/3}}{n_{\text{rms},3}^{2/3}} T_4^{0.28} \text{ cm} \quad (12)$$

be the radius of a dustless Strömgren sphere with density  $n_{\text{rms}}$ . The actual radius of the ionized zone is  $R = y_{\text{max}}\lambda_0 < R_{s0}$ , and the fraction of the  $h\nu > 13.6 \text{ eV}$  photons that are absorbed by H is simply

$$f_{\text{ion}} = \left( \frac{R}{R_{s0}} \right)^3 \quad . \quad (13)$$

For given  $(\beta, \gamma)$ , varying the initial value<sup>1</sup> of  $u = n_0/n$  at some fixed  $y = r/\lambda_0$  generates solutions with different density profiles. Therefore the full set of solutions forms a three-parameter family of similarity solutions  $u(y)$ ,  $\phi(y)$ , and  $\tau(y)$ , parametrized by  $\beta$ ,  $\gamma$ , and a third parameter. The third parameter can be taken to be  $Q_0 n_{\text{rms}}$ . For dusty H II regions, an alternative choice for the third parameter is the dust optical depth on a path  $R_{s0}$  with density  $n_{\text{rms}}$ :

$$\tau_{d,0} \equiv n_{\text{rms}} R_{s0} \sigma_d = 2.10 (Q_{0,49} n_{\text{rms},3})^{1/3} T_4^{0.28} \frac{\sigma_d}{10^{-21} \text{ cm}^2} \quad (14)$$

$$= 0.188 \gamma (Q_{0,49} n_{\text{rms},3})^{1/3} T_4^{-1.55} \frac{\langle h\nu \rangle_i}{18 \text{ eV}}. \quad (15)$$

### 3. Results

Equations (8-10) can be integrated numerically. Figure 2a shows the solution for the case where no dust is present ( $\gamma = 0$ ). Radiation pressure associated with photoionization produces a density gradient in the H II region, but it is modest unless  $Q_0 n_{\text{rms}}$  is very large, and the central density is nonzero. For a single O-type star with  $Q_{0,49} \approx 1$ , the density is uniform to within  $\pm 15\%$  provided  $n_{\text{rms}} \lesssim 10^3 \text{ cm}^{-3}$ .

If dust is present in the gas, with abundance (relative to H) and properties characteristic of the diffuse ISM, the parameter  $\gamma \approx 15$ . Density profiles are shown in Fig. 2b-d for  $\beta = 3$  and  $\gamma = 5, 10, 20$ , corresponding approximately to  $\sigma_d = 0.5, 1, 2 \times 10^{-21} \text{ cm}^2$ . With dust present, the density goes to zero at  $r = 0$ , but the size of the low-density central cavity (as a fraction of the radius  $R$  of the ionization front) increases as  $Q_0 n_{\text{rms}}$  increases. The enhancement of the density near the ionization front also becomes more pronounced as  $Q_0 n_{\text{rms}}$  is increased. For  $Q_{0,49} n_{\text{rms}} = 10^5 \text{ cm}^{-3}$ ,  $n(R) = 2.5 n_{\text{rms}}$ .

The emission measure  $EM(b) = \int n_e^2 ds$  is shown as a function of impact parameter  $b$  in Figure 3. For small values of  $Q_0 n_{\text{rms}}$ , the intensity profile is close to the semicircular profile of a uniform density sphere. As  $Q_0 n_{\text{rms}}$  is increased, the profile becomes flattened, but only begins to develop an appreciable central minimum for  $Q_{0,49} n_{\text{rms}} \gtrsim 10^{4.5} \text{ cm}^{-3}$ .

When dust is present, however, the profiles are strongly affected. For standard parameters  $\beta = 3, \gamma = 10$ , the emission measure shows a pronounced central minimum for  $Q_{0,49} n_{\text{rms}} \gtrsim 10^3 \text{ cm}^{-3}$ , with a peak-to-minimum ratio  $> 2$  for  $Q_{0,49} n_{\text{rms}} \gtrsim 10^4 \text{ cm}^{-3}$ . As  $Q_0 n_{\text{rms}}$  is increased, the ionized gas becomes concentrated in a thin, dense shell, the peak intensity near the edge rises, and the central emission measure changes from  $EM(0) = 2n_{\text{rms}}^2 R$  for small  $Q_0 n_{\text{rms}}$  to  $EM(0) \rightarrow (2/3)n_{\text{rms}}^2 R$  as  $Q_0 n_{\text{rms}} \rightarrow \infty$ .

Figure 4(a) shows  $f_{\text{ion}}$ , the fraction of the  $h\nu > 13.6 \text{ eV}$  photons emitted by the star that photoionize H (i.e., are not absorbed by dust), as a function of the parameter  $\tau_{d0}$ . Results are

---

<sup>1</sup> For  $\gamma > 0$ ,  $u \propto \exp[(\beta + 1)\gamma/y] \rightarrow \infty$  as  $y \rightarrow 0$ , and the integration must start at some small  $y > 0$ .

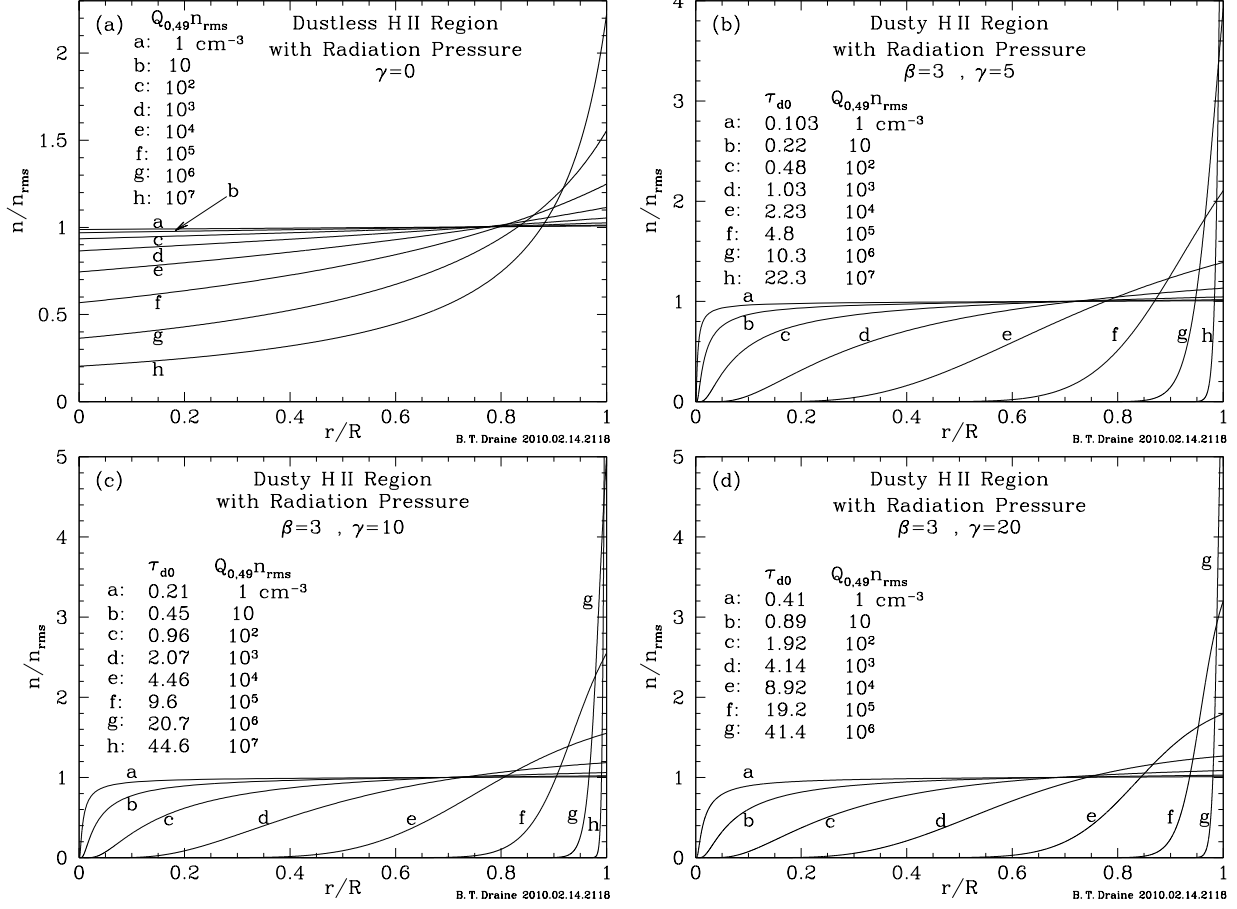


Fig. 2.— Normalized density profiles of static equilibrium H II regions, as a function of  $r/R$ , where  $R$  is the radius of the ionized region. Profiles are shown for 7 values of  $Q_0 n_{\text{rms}}$ ; the numerical values given in the legends assume  $T_4 = 0.94$  and  $\langle h\nu \rangle_i = 18 \text{ eV}$ . (a) Dustless ( $\gamma = 0$ ); (b)  $\gamma = 5$ ; (c)  $\gamma = 10$ ; (d)  $\gamma = 20$ .

shown for  $\beta = 2, 3, 5$  and  $\gamma = 5, 10, 20$ . For  $2 \leq \beta \leq 5$ ,  $5 \leq \gamma \leq 20$ , and  $0 \leq \tau_{d0} \leq 40$ , the numerical results in Figure 4(a) can be approximated by the fitting formula

$$f_{\text{ion}}(\beta, \gamma, \tau_{d0}) \approx \frac{1}{1 + (2/3 + AB)\tau_{d0}} + \frac{AB\tau_{d0}}{1 + B\tau_{d0}} \quad (16)$$

$$A = \frac{1}{1 + 0.75\gamma^{0.65}\beta^{-0.44}} \quad (17)$$

$$B = \frac{0.5}{1 + 0.1(\gamma/\beta)^{1.5}} \quad (18)$$

where  $\beta$ ,  $\gamma$ , and  $\tau_{d0}$  are given by (6), (7), and (14). The form of eq. (16-18) has no physical significance, but eq. (16) can be used to estimate the total H ionization rate  $f_{\text{ion}}Q_0$  in dusty H II regions.

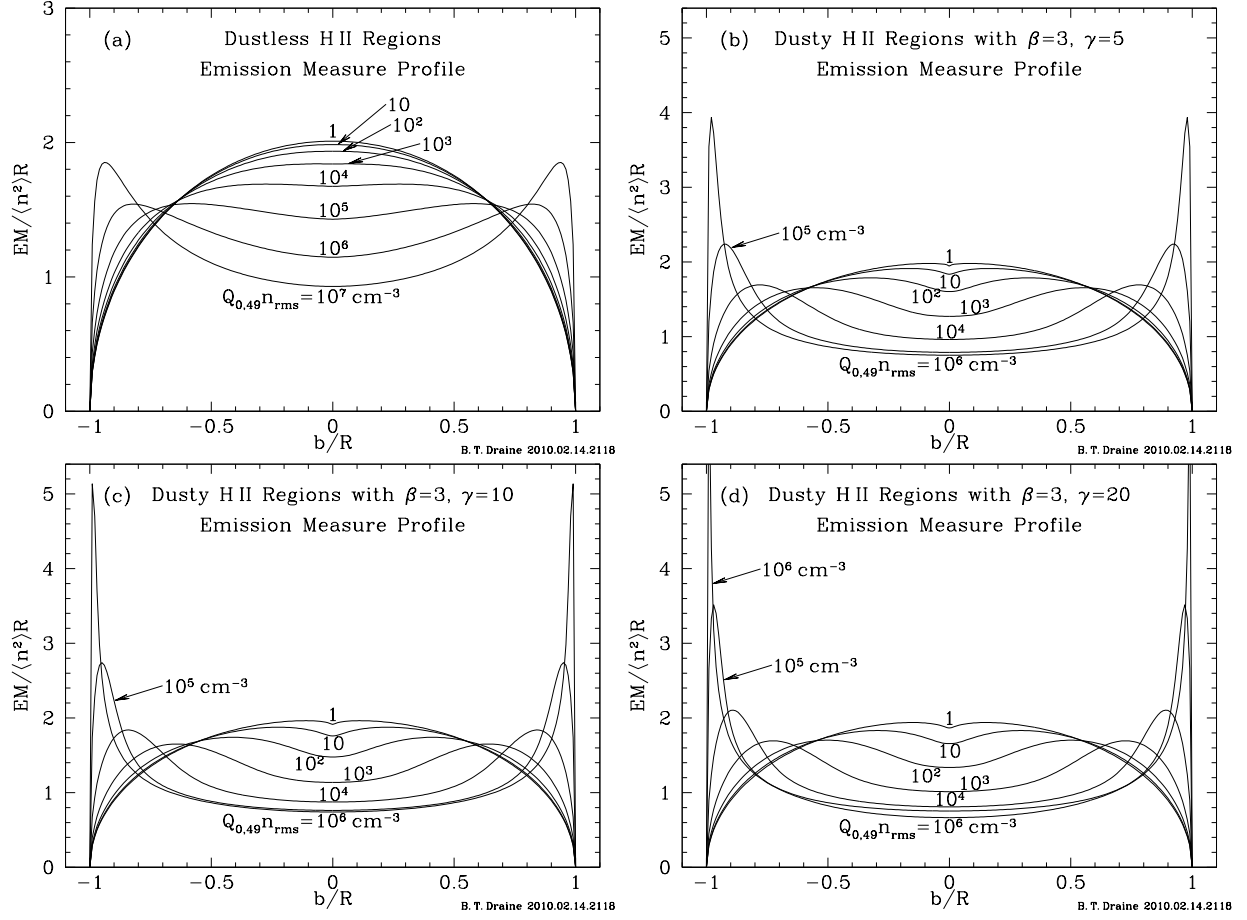


Fig. 3.— Normalized emission measure (EM) profiles for a cut across the center of H II regions with (a)  $\gamma = 0$  (no dust), (b)  $\gamma = 5$ , (c)  $\gamma = 10$ , and (d)  $\gamma = 20$ . Profiles are shown for selected values of  $Q_0 n_{\text{rms}}$ . Numerical values of  $Q_{0,49} n_{\text{rms}}$  assume  $T = 9400 \text{ K}$  and  $\langle h\nu \rangle_i = 18 \text{ eV}$ .

Even for large values of  $\tau_{d0}$ , Fig. 4 shows that  $\sim 1/3$  of the  $h\nu > 13.6 \text{ eV}$  photons are absorbed by hydrogen. This contrasts with the uniform-density models of Petrosian et al. (1972), where the fraction of the  $h\nu > 13.6 \text{ eV}$  photons that are absorbed by the gas goes to zero as  $\tau_{d0}$  becomes large. When  $\tau_{d0} \gg 1$ , the present models have the gas and dust concentrated in a thin, dense, shell. Because the shell is dense, radiative recombination is rapid, the neutral hydrogen fraction is enhanced, and H atoms can compete with dust to absorb  $h\nu > 13.6 \text{ eV}$  photons. In the low density limit  $Q_0 n_{\text{rms}} \rightarrow 0$ , the actual optical depth from center to edge  $\tau(R) \approx \tau_{d0}$ , but when  $Q_0 n_{\text{rms}}$  becomes large,  $\tau(R)$ , shown in Fig. 4b, becomes significantly smaller than  $\tau_{d0}$ .

The density contrast is shown in Fig. 4(c), showing the ratio of the density just inside the edge to the r.m.s. density. As  $\tau_{d0}$  increases, this ratio continues to increase. The ratio of the peak emission measure to the central emission measure is plotted in Fig. 4(d), showing that this, too,



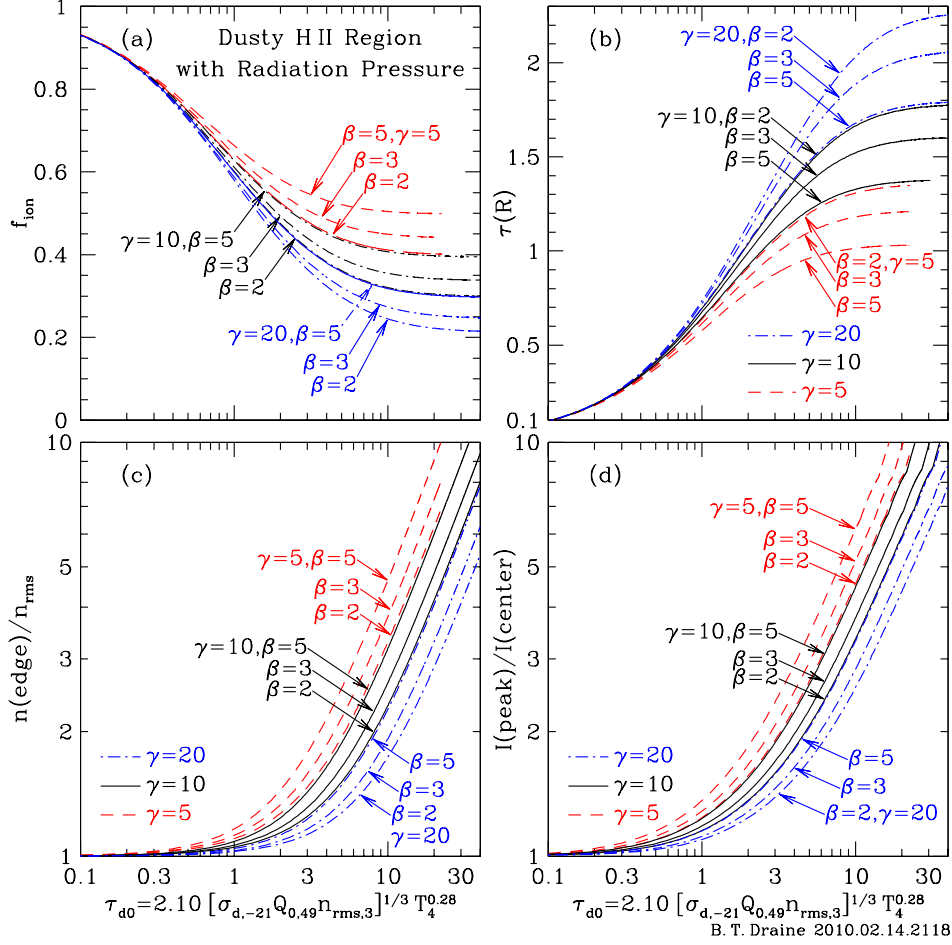


Fig. 4.— For dusty H II regions with  $\gamma = 5, 10, 20$  and  $\beta = 2, 3, 5$ : (a) fraction of the  $h\nu > 13.6$  eV photons that photoionize H in dusty H II regions with radiation pressure, as a function of  $\tau_{d0}$ ; (b) center-to-edge dust optical depth  $\tau(R)$ ; (c) ratio  $n(R)/n_{\text{rms}}$  of the edge density to the rms density; (d) ratio of peak emission measure/central emission measure. The dotted lines in (a) show the fitting formula (16) for  $(\beta, \gamma) = (5, 5), (5, 10),$  and  $(2, 20)$ .

becomes large as  $\tau_{d0}$  is increased.

## 4. Dust Drift

### 4.1. Gas Drag vs. Radiation Pressure

Eq. (1) assumes the dust to be tightly coupled to the gas, so that the radiation pressure force on the dust can be considered to act directly on the gas. In reality, radiation pressure will drive the

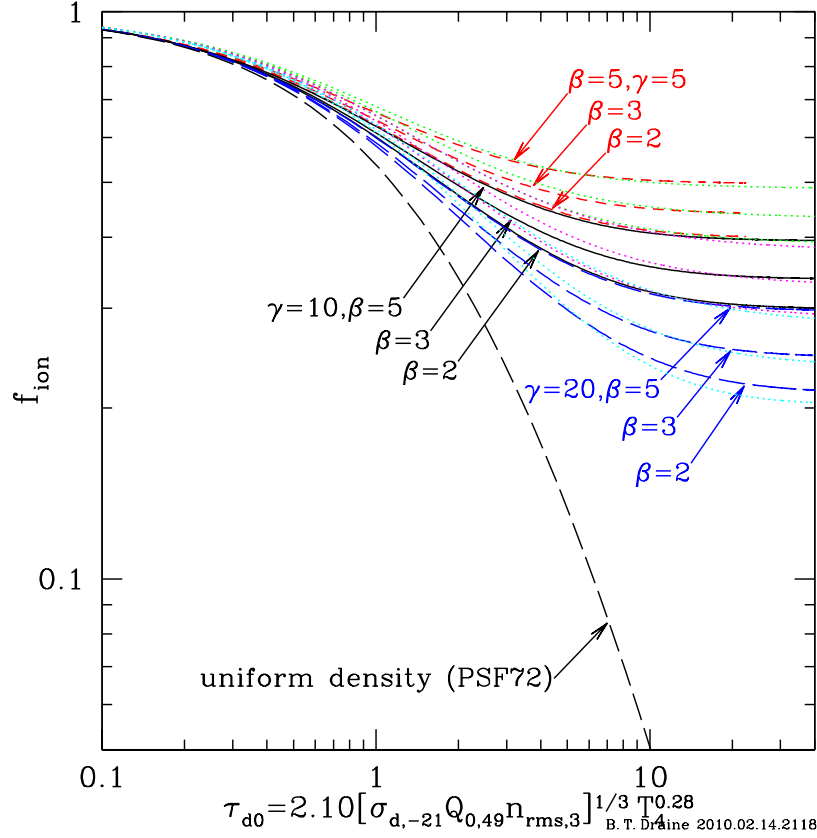


Fig. 5.— Fraction  $f_{\text{ion}}$  of the  $h\nu > 13.6\text{ eV}$  photons that photoionize H in dusty H II regions with radiation pressure, as a function of  $\tau_{d0}$ , for  $\beta = 2, 3, 5$  and  $\gamma = 5, 10, 20$ . The dotted lines in (a) show the fitting formula (16) for each case shown. Also shown is  $f_{\text{ion}}$  calculated for assumed uniform density (Petrosian et al. 1972).

dust grains through the plasma. If the grains approach their terminal velocities (i.e., acceleration can be neglected) then, as before, it can be assumed that the radiation pressure force is effectively applied to the gas. However, the motion of the dust grains will lead to changes in the dust/gas ratio, due to movement of the grains from one zone to another, as well as because of grain destruction. Here we estimate the drift velocities of grains.

Let  $Q_{\text{pr}}\pi a^2$  be the radiation pressure cross section for a grain of radius  $a$ . Figure 6 shows  $Q_{\text{pr}}(a)$  averaged over blackbody radiation fields with  $T = 25000\text{ K}$ ,  $32000\text{ K}$ , and  $40000\text{ K}$ , for carbonaceous grains and amorphous silicate grains. For spectra characteristic of O stars,  $\langle Q_{\text{pr}} \rangle \approx 1.5$  for  $0.02\mu\text{m} \lesssim a \lesssim 0.25\mu\text{m}$ .

If the magnetic field  $B = 0$ , the terminal velocity  $v_d$  for a grain at distance  $r$  is determined by

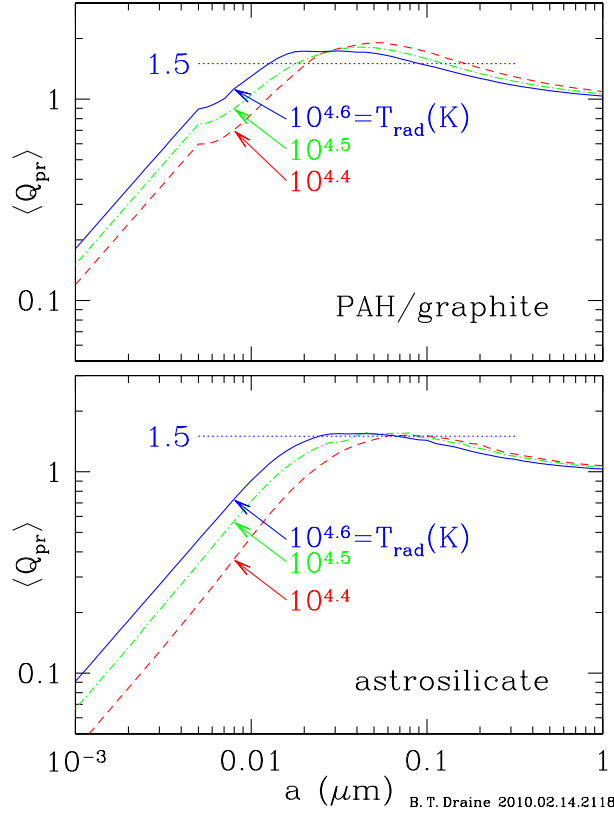


Fig. 6.— Spectrum-averaged radiation pressure efficiency factor  $\langle Q_{\text{pr}} \rangle$  as a function of radius, for  $T = 25000 \text{ K}$ ,  $32000 \text{ K}$ , and  $40000 \text{ K}$  blackbody spectra. For temperatures characteristic of O stars,  $\langle Q_{\text{pr}} \rangle \approx 1.5$  to within 20% for  $0.02 \mu\text{m} \lesssim a \lesssim 0.25 \mu\text{m}$ .

balancing the forces due to radiation pressure and gas drag:

$$\frac{L(r)}{4\pi r^2 c} \pi a^2 \langle Q_{\text{pr}} \rangle = 2\pi a^2 n k T G(s) \quad , \quad s \equiv \frac{v_d}{\sqrt{2kT/m_{\text{H}}}} \quad , \quad (19)$$

where the drag function  $G(s)$ , including both collisional drag and Coulomb drag, can be approximated by (Draine & Salpeter 1979)

$$G(s) \approx \frac{8s}{3\sqrt{\pi}} \left( 1 + \frac{9\pi}{64} s^2 \right)^{1/2} + \left( \frac{eU}{kT} \right)^2 \ln \Lambda \frac{s}{(3\sqrt{\pi}/4 + s^3)} \quad , \quad (20)$$

$$\Lambda = \frac{3}{2ae} \frac{kT}{|eU|} \left( \frac{kT}{\pi n_e} \right)^{1/2} = 6.6 \times 10^6 a_{-5}^{-1} \frac{kT}{|eU|} T_4^{1/2} n_3^{-1/2} \quad , \quad (21)$$

where  $U$  is the grain potential,  $a_{-5} \equiv a/10^{-5} \text{ cm}$ , and  $n_3 \equiv n_e/10^3 \text{ cm}^{-3}$ . The charge on the grains will be determined by collisional charging and photoelectric emission. Collisional charging would result in  $eU/kT \approx -2.51$  (Spitzer 1968), or  $U \approx -2.16 T_4 \text{ V}$ . Photoelectric charging will dominate

close to the star, but is expected to result in potentials of  $U \lesssim 10\text{V}$ . Taking  $|eU/kT| \approx 2.5$  and  $\ln \Lambda \approx 14.8$  as representative,

$$G(s) \approx \left[ 1.50 \left( 1 + \frac{9\pi}{64} s^2 \right)^{1/2} + \frac{69.5}{1 + 4s^3/3\sqrt{\pi}} \right] s \quad . \quad (22)$$

Note that  $G(s)$  is not monotonic: as  $s$  increases from 0,  $G(s)$  reaches a peak value  $\sim 42$  for  $s \approx 0.89$ , but then begins to decline with increasing  $s$  as the Coulomb drag contribution falls. At sufficiently large  $s$ , the direct collisional term becomes large enough that  $G(s)$  rises above  $\sim 42$  and continues to rise thereafter.

The drag time for a grain of density  $\rho = 3 \text{ g cm}^{-3}$  in H II gas is

$$\tau_{\text{drag}} = \frac{Mv}{F_{\text{drag}}} = 295 \left( \frac{a_{-5}}{n_3 T_4^{1/2}} \right) \frac{s}{G(s)} \text{ yr} \quad . \quad (23)$$

For  $n_3 \gtrsim 0.01$  this is sufficiently short that each grain can be assumed to be moving at its terminal velocity  $v_d$ , with isothermal Mach number  $s \equiv v_d / \sqrt{2kT/m_H}$  determined by the dimensionless equation

$$G(s) = \left[ \phi(y) + \beta e^{-\tau(y)} \right] \frac{u(y)}{y^2} \langle Q_{\text{pr}} \rangle \quad , \quad y \equiv \frac{r}{\lambda_0} \quad . \quad (24)$$

Eq. (24) is solved to find  $s(r)$ . For  $20 < G < 42$ , there are three values of  $s$  for which the drag force balances the radiation pressure force. The intermediate solution is unstable; we choose the smaller solution,<sup>2</sup> which means that  $s$  undergoes a discontinuous jump from  $\sim 0.9$  to  $6.2$  at  $G \approx 42$ . The resulting terminal velocity  $v(r)$  is shown in Figure 7 for 7 values of  $Q_{0,49} n_{\text{rms}}$ . The velocities in the interior can be very large, but the velocities where most of the dust is located [ $\tau(r)/\tau(R) > 0.5$ ] are much smaller.

In the outer part of the bubble, where most of the gas and dust are located, the drift velocities are much more modest. This is visible in Fig. 7a, where the drift speeds become small as  $r \rightarrow R$ , but is more clearly seen in Fig. 7b, showing drift speeds as a function of normalized optical depth. The range  $0.5 < \tau(r)/\tau(R) < 1$  contains more than 50% of the dust, and throughout this zone the drift speeds are  $\lesssim 0.3 \text{ km s}^{-1}$  even for  $Q_{0,49} n_{\text{rms}}$  as large as  $10^7 \text{ cm}^{-3}$ . With drift speeds  $v_d \lesssim 0.3 \text{ km s}^{-1}$ , grains will not be destroyed, except perhaps by shattering in occasional collisions between grains with different drift speeds. However, for large values of  $n_{\text{rms}}$ , these grains are located close to the boundary, the drift times may be short, and the grains may be driven out of the H II and into the surrounding shell of dense neutral gas. This will be discussed further below.

---

<sup>2</sup> This solution is physically relevant if the drift speed began with  $s \lesssim 0.9$  and increased with time.

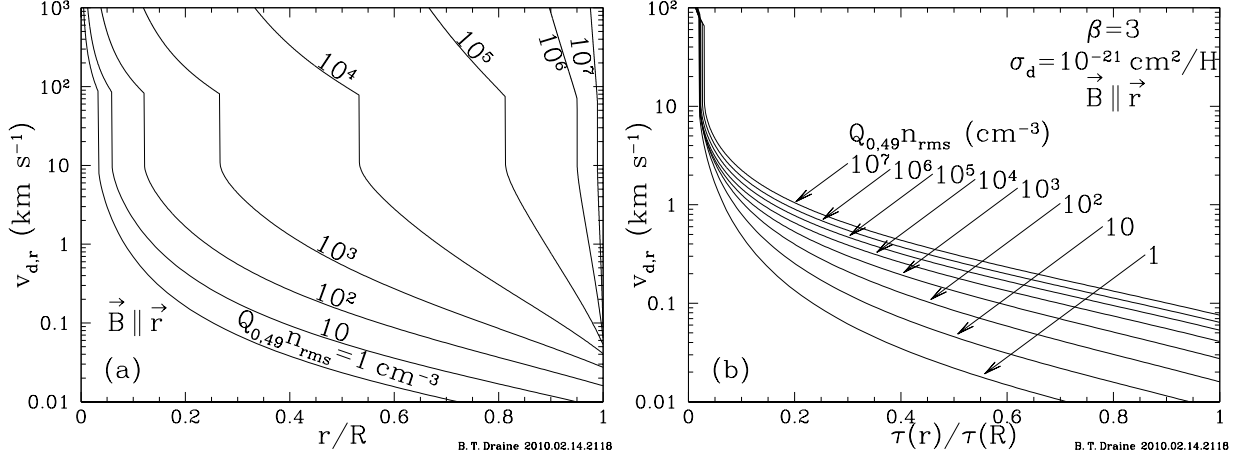


Fig. 7.— Radial drift velocities  $v_{d,r}$  for six different H II regions, all with  $\beta = 3$  and  $\gamma = 10$ , for  $Q_{\text{pr}} = 1.5$ ,  $|eU/kT| = 2.5$ , and  $B = 0$ . (a)  $v_{d,r}$  vs  $r/R$ . All solutions have large drift velocities near the center, which will result in removal of the dust from the interior. Drift velocities increase with increasing  $Q_0 n_{\text{rms}}$ . (b)  $v_{d,r}$  as a function of normalized dust column density  $\tau(r)/\tau(R)$ . In regions where most of the dust is concentrated, drift velocities are low.

## 4.2. Magnetic Fields

Let  $\epsilon_B \equiv B^2/16\pi nkT$  be the ratio of magnetic pressure to gas pressure. The importance of magnetic fields for the grain dynamics is determined by the dimensionless ratio  $\omega\tau_{\text{drag}}$ , where  $\omega \equiv QB/Mc$  is the gyrofrequency for a grain with charge  $Q$  and mass  $M$  in a magnetic field  $B$ :

$$(\omega\tau_{\text{drag}})^2 = 17.3 \frac{T_4^2}{n_3 a_{-5}^2} \left( \frac{\epsilon_B}{0.1} \right) \left( \frac{eU/kT}{2.5} \right)^2 \left( \frac{71}{G(s)/s} \right)^2, \quad \epsilon_B \equiv \left( \frac{B^2/8\pi}{2nkT} \right). \quad (25)$$

If  $|eU/kT| \approx 2.5$  and  $\ln \Lambda \approx 15$ , then  $(G(s)/s) \approx 71$  for  $s \lesssim 0.5$ .

Let the local magnetic field be  $\mathbf{B} = B(\hat{\mathbf{r}} \cos \theta + \hat{\mathbf{y}} \sin \theta)$ . The steady-state drift velocity is

$$v_d = \left( \frac{F_{\text{rad}}\tau_{\text{drag}}}{M} \right) \sqrt{\frac{1 + (\omega\tau_{\text{drag}})^2 \cos^2 \theta}{1 + (\omega\tau_{\text{drag}})^2}}, \quad (26)$$

$$v_{d,r} = \left( \frac{F_{\text{rad}}\tau_{\text{drag}}}{M} \right) \frac{1 + (\omega\tau_{\text{drag}})^2 \cos^2 \theta}{1 + (\omega\tau_{\text{drag}})^2}, \quad (27)$$

$$v_{d,y} = \left( \frac{F_{\text{rad}}\tau_{\text{drag}}}{M} \right) \frac{(\omega\tau_{\text{drag}})^2 \sin \theta \cos \theta}{1 + (\omega\tau_{\text{drag}})^2}, \quad (28)$$

$$v_{d,z} = - \left( \frac{F_{\text{rad}}\tau_{\text{drag}}}{M} \right) \frac{\omega\tau_{\text{drag}} \sin \theta}{1 + (\omega\tau_{\text{drag}})^2}, \quad (29)$$

where  $v_{d,r}$ ,  $v_{d,y}$ ,  $v_{d,z}$  are the radial and transverse components. If  $\sin \theta \rightarrow 0$ , the magnetic field does not affect the radiation-pressure-driven drift velocity, but in the limit  $\sin \theta \rightarrow 1$  magnetic effects can strongly suppress the radial drift if  $\omega\tau_{\text{drag}} \gg 1$  and  $\cos \theta \ll 1$ .

The magnetic field strength is uncertain, but it is unlikely that the magnetic energy density will be comparable to the gas pressure; hence  $\epsilon_B \lesssim 0.1$ . From eq. (25) it is then apparent that if the magnetic field is strong ( $\epsilon_B \approx 0.1$ ), magnetic effects on the grain dynamics can be important in low density H II regions, but will not be important for very high densities:  $(\omega\tau_{\text{drag}})^2 \lesssim 1$  for  $n_3 \gtrsim 170a_{-5}^{-2}\epsilon_B$ .

### 4.3. Drift Timescale

When radiation pressure effects are important, the gas and dust are concentrated in a shell that becomes increasingly thin as  $Q_0 n_{\text{rms}}$  is increased. The drift velocities where most of the dust is located are not large (see Fig. 7b), but the grains are also not far from the ionization front. The timescale on which dust drift would be important can be estimated by calculating the drift velocity at the radius  $r_{0.5}$  defined by  $\tau(r_{0.5}) = 0.5\tau(R)$ . More than 50% of the dust has  $r_{0.5} < r < R$ . Figure 8 shows the characteristic drift time

$$t_{\text{drift}} \equiv \frac{R - r_{0.5}}{v_{d,r}(r_{0.5})} \quad . \quad (30)$$

If no magnetic field is present, the drift velocity depends only on  $T$  and the dimensionless quantities  $\{\phi, \tau, u, y, \langle Q_{\text{pr}} \rangle\}$  (see eq. 24). It is easy to see that for fixed  $T$  and  $Q_0 n_{\text{rms}}$ , the radius  $R \propto Q_0$ , thus  $t_{\text{drift}} \propto Q_0$ . Figure 8 shows  $t_{\text{drift}}/Q_{0,49}$ . For  $Q_{0,49} = 1$ , H II regions with  $n_{\text{rms}} \gtrsim 10^3 \text{ cm}^{-3}$  have  $t_{\text{drift}} < 10^6 \text{ yr}$  if magnetic effects are negligible. If the magnetic field is strong ( $\epsilon_B \approx 0.1$ ), then small grains ( $a \lesssim 0.03 \mu\text{m}$ ) have  $t_{\text{drift}} < 10^6 \text{ yr}$  only for  $n_{\text{rms}} \gtrsim 5 \times 10^3 \text{ cm}^{-3}$ .

### 4.4. Grain Destruction

Arthur et al. (2004) computed models of uniform density H II regions including the effects of dust destruction by sublimation or evaporation, finding that the dust/gas ratio can be substantially reduced near the star. If the maximum temperature at which a grain can survive is  $T_{\text{sub}}$ , and the Planck-averaged absorption efficiencies are  $Q_{\text{uv}}$  and  $Q_{\text{ir}}$  for  $T = T_\star$  and  $T = T_{\text{max}}$ , then grains will be destroyed within a distance  $r_{\text{sub}}$  with

$$\frac{r_{\text{sub}}}{R_{s0}} = 2.82 \times 10^{-3} L_{39}^{1/6} n_{\text{rms},3}^{2/3} \left( \frac{10^3 \text{ K}}{T_{\text{sub}}} \right)^2 \left( \frac{L_{39}}{Q_{0,49}} \right)^{1/3} \left( \frac{Q_{\text{uv}}/Q_{\text{ir}}}{10^2} \right)^{1/2} \quad (31)$$

For parameters of interest (e.g.,  $L_{39}/Q_{0,49} \approx 1$ ,  $L_{39} \lesssim 10^2$ )  $r_{\text{sub}}/R_{s0} \ll 1$  for  $n_{\text{rms}} \lesssim 10^5 \text{ cm}^{-3}$ , and sublimation would therefore destroy only a small fraction of the dust.

As we have seen, we expect radiation pressure to create a Drift velocities  $v_d \gtrsim 75 \text{ km s}^{-1}$  will lead to sputtering by impacting He ions, with sputtering yield  $Y(\text{He}) \approx 0.2$  for  $80 \lesssim v \lesssim 500 \text{ km s}^{-1}$  (Draine 1995). For hypersonic motion, the grain of initial radius  $a$  will be destroyed after traversing

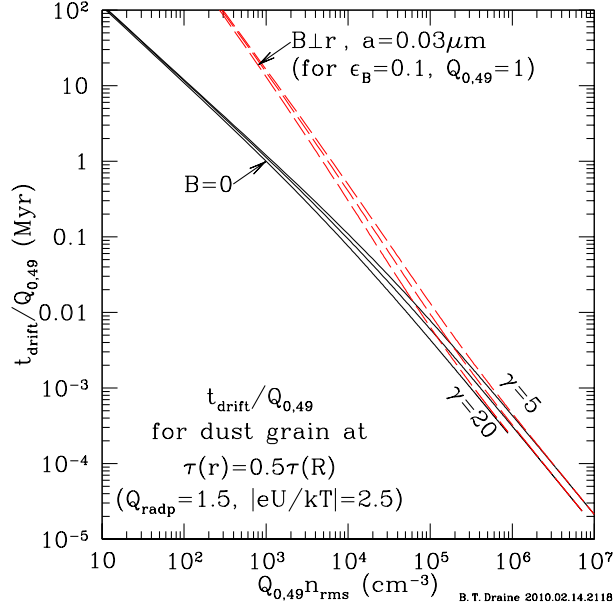


Fig. 8.— Drift timescale  $t_{\text{drift}}/Q_{0.49}$  (see eq. 30) for  $\beta = 3$  and  $\gamma = 5, 10$ , and  $20$ . The dust grains are assumed to have  $Q_{\text{pr}} = 1.5$  and  $|eU/kT| = 2.5$ . Solid lines are for  $B = 0$  (or  $\mathbf{B} \parallel \mathbf{r}$ ). Broken lines are for  $\mathbf{B} \perp \mathbf{r}$  with  $\epsilon_B = 0.1$ ,  $a = 0.03\mu\text{m}$ , and  $Q_{0.49} = 1$ .

a column density

$$n_{\text{H}}\Delta r = \frac{n_{\text{H}}}{n_{\text{He}}} \frac{4\rho a}{Y(\text{He})\mu} \approx 2 \times 10^{20} a_{-5} \left( \frac{Y(\text{He})}{0.2} \right) \text{ cm}^{-2} \quad (32)$$

for a grain density  $\rho/\mu = 1 \times 10^{23} \text{ cm}^{-3}$ , appropriate for either silicates (e.g.,  $\text{FeMgSiO}_4$ ,  $3.8 \text{ g cm}^{-3}/25m_{\text{H}} = 9 \times 10^{22} \text{ cm}^{-3}$ ) or carbonaceous material ( $2 \text{ g cm}^{-3}/12m_{\text{H}} = 1.0 \times 10^{23} \text{ cm}^{-3}$ ). Therefore the dust grain must traverse

$$\Delta\tau_d = \sigma_d n_{\text{H}} \Delta r = 0.2 \sigma_{d,-21} a_{-5} \left( \frac{Y(\text{He})}{0.2} \right) \quad (33)$$

if it is to be substantially eroded by sputtering.

## 5. Discussion

### 5.1. Absorption of Ionizing Photons by Dust

For a sample of 13 Galactic H II regions, Inoue (2002) used infrared and radio continuum observations to obtain the values of  $f_{\text{ion}}$  shown in Figure 9. The estimated values of  $f_{\text{ion}}$  are much larger than would be expected for uniform H II regions with dust-to-gas ratios comparable to the values found in neutral clouds. Inoue (2002) concluded that the central regions of these H II regions must be dust-free, noting that this was likely to be due to the combined effects of stellar winds

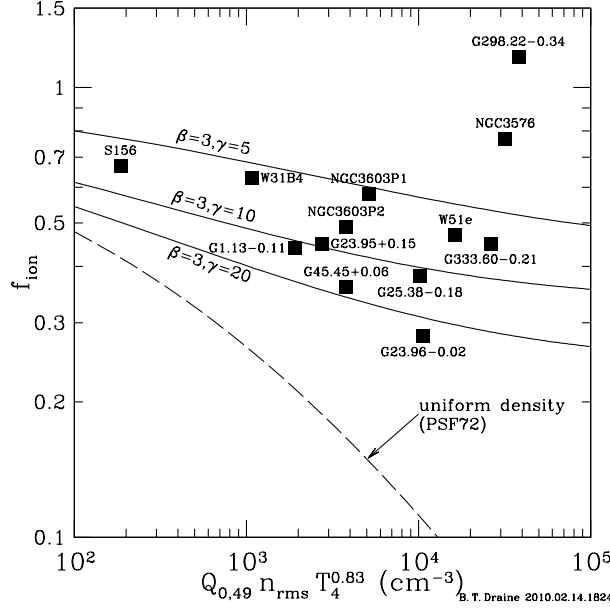


Fig. 9.— Photoionizing fraction  $f_{\text{ion}}$  for 12 Galactic H II regions, as estimated by Inoue (2002) from infrared and radio observations, vs.  $Q_{0,49}n_{\text{rms}}T_4^{0.83}$  (see text).  $f_{\text{ion}}$  cannot exceed 1, therefore the high values found for G298.22-0.34 give some indication of the uncertainties in estimation of  $f_{\text{ion}}$ . Solid lines:  $f_{\text{ion}}$  for H II regions with radiation pressure. Broken line:  $f_{\text{ion}}$  for uniform H II regions with  $\sigma_d = 10^{-21} \text{ cm}^2 \text{ H}^{-1}$ .

and radiation pressure on dust. As seen in Fig. 9, the values of  $f_{\text{ion}}$  found by Inoue are entirely consistent to what is expected for H II regions in equilibrium with radiation pressure for  $5 \lesssim \gamma \lesssim 20$ , corresponding to  $0.5 \lesssim \sigma_{d,-21} \lesssim 2$ , with no need to appeal to stellar winds or grain destruction.

## 5.2. Cavities in H II Regions: N49

Even without dust present, radiation pressure from photoionization can alter the density profile in a static H II region, lowering the central density and enhancing the density near the edge of the ionized region (see Fig. 2a). As seen in Figure 3a, for large values of  $Q_0 n_{\text{rms}}$  the surface brightness profile can be noticeably flattened. If dust is assumed to be present, with properties typical of the dust in diffuse clouds, the equilibrium density profile changes dramatically, with central cavity surrounded by a high-pressure shell of ionized gas held off by radiation pressure. In real H II regions, fast stellar winds will also act to inflate a low-density cavity, or “bubble”, near the star; the observed density profile will be the combined result of the stellar wind bubble and the effects of radiation pressure.

The GLIMPSE survey (Churchwell et al. 2009) has discovered and catalogued numerous in-



terstellar “bubbles”. An example is N49 (Watson et al. 2008), with a ring of free-free continuum emission at 20 cm, surrounded by a ring of  $8\mu\text{m}$  PAH emission. An O6.5V star is located near the center of the N49 ring. The image is nearly circularly symmetric, with only a modest asymmetry that could be due to motion of the star relative to the gas. The 20 cm image has a ring-peak-to-center intensity ratio  $I(\text{peak})/I(\text{center}) \approx 2$ .

Is the density profile in N49 consistent with what is expected for radiation pressure acting on dust? From the 2.89 Jy flux from N49 at  $\lambda = 20$  cm (Helfand et al. 2006) and distance  $5.7 \pm 0.6$  kpc (Churchwell et al. 2006), the stellar source has  $Q_{0,49} \approx (0.78 \pm 0.16)/f_{\text{ion}}$ . If  $f_{\text{ion}} \approx 0.6$ , then  $Q_{0,49} \approx (1.3 \pm 0.3)$ . The H II region, with radius  $(0.018 \pm 0.02)$  deg, has  $n_{\text{rms}} \approx 197 \pm 63 \text{ cm}^{-3}$ . Hence  $Q_{0,49}n_{\text{rms}} \approx 260 \text{ cm}^{-3}$ . If  $\sigma_{d,-21} = 1$ , then  $\tau_{d0} \approx 1.3$ . From Fig. 4a we confirm that  $f_{\text{ion}} \approx 0.6$  for  $\tau_{d0} \approx 1.3$ .

Figure 4d shows that an H II region with  $\tau_{d0} = 1.3$  is expected to have a central minimum in the emission measure, but with  $I(\text{peak})/I(\text{center}) \approx 1.3$  for  $\beta = 3, \gamma = 10$ , whereas the observed  $I(\text{peak})/I(\text{center}) \approx 2$ . The central cavity in N49 is therefore significantly larger than would be expected based on radiation pressure alone. While the effects of radiation pressure are not negligible in N49, the observed cavity must be the result of the combined effects of radiation pressure and a dynamically-important stellar wind (which is of course not unexpected for an O6.5V star).

### 5.3. Extreme Values of $Q_0 n_{\text{rms}}$ : The Arches Cluster

H II regions powered by dense clusters of OB stars can have very large values of  $Q_0 n_{\text{rms}}$ . For example, the Arches cluster, with  $Q_{0,49} \approx 400$  (Figer et al. 2002) and  $n_{\text{rms}} \approx 2 \times 10^4 \text{ cm}^{-3}$  (Krumholz & Matzner 2009) has  $Q_{0,49}n_{\text{rms}} \approx 10^7 \text{ cm}^{-3}$ . For these parameters, we have  $\tau_{d0} \approx 40$ , and the solution has  $\tau(R) \approx 1.6$  and  $f_{\text{ion}} \approx 0.34$  (cf. Fig. 4a,b with  $\beta = 3, \gamma = 10$ ). If the H II region were static, the time  $t_{\text{drift}}$  for dust to escape would be only  $\sim 10^4$  yr (see Fig. 8), but it is likely that the ionization front is propagating too rapidly for dust to drift outwards into the neutral gas.

The region with drift velocities  $v_{d,r} \gtrsim 100 \text{ km s}^{-1}$  would have  $\Delta\tau \approx 0.03\tau(R)$  (see Fig. 7b) hence  $\Delta\tau \approx 0.05$ . Therefore the region over which high velocity drift occurs is too short for sputtering to substantially erode a typical grain with  $a_{-5} \gtrsim 1$ . The dust-to-gas ratio in the low-density central zone will be lowered by the radial dust drift, but the region so affected contains only a small fraction of the ionized gas.

### 5.4. Lyman- $\alpha$

The original ionizing photon deposits a radial momentum  $h\nu_i/c$  at the point where it is absorbed by either a neutral atom or a dust grain. A fraction  $(1 - f_{\text{ion}})$  of the ionizing photons are

absorbed by dust; this energy is reradiated isotropically, with no additional force exerted on the emitting material. Because the infrared optical depth within the H II region is small, the infrared emission escapes freely, with no dynamical effect within the H II region.

A fraction  $f_{\text{ion}}$  of the ionizing energy is absorbed by the gas. Subsequent radiative recombination and radiative cooling converts this energy to photons, but the isotropic emission process itself involves no net momentum transfer to the gas. We have seen above that the H II can have a center-to-edge optical depth  $\tau(R) \approx 1.6$  for  $\tau_{d0} \gtrsim 5$ , or  $Q_{0,49}n_{\text{rms}} \gtrsim 10^2 \text{ cm}^{-3}$  (cf. Fig. 4b with  $\beta = 3$ ,  $\gamma = 10$ ). This optical depth applies to the  $h\nu > 13.6 \text{ eV}$  ionizing radiation; the center-to-edge optical depth for the  $h\nu < 3.4 \text{ eV}$  Balmer lines and collisionally-excited cooling lines within the ionized zone will be significantly smaller, and much of this radiation will escape dust absorption or scattering within the H II region. That which is absorbed or scattered will exert a force on the dust at that point only to the extent that the radiation field is anisotropic. We conclude that momentum deposition from the Balmer lines and collisionally-excited cooling lines will be negligible within the ionized zone.

Lyman- $\alpha$  is a special case. At low densities ( $n \ll 10^3 \text{ cm}^{-3}$ ),  $\sim 70\%$  of Case B recombinations result in emission of a Ly- $\alpha$  photon, increasing to  $> 95\%$  for  $n > 10^4 \text{ cm}^{-3}$  as a result of collisionally-induced  $2s \rightarrow 2p$  transitions (Brown & Mathews 1970). After being emitted isotropically, the photon may scatter many times before either escaping from the H II or being absorbed by dust. Most of the scatterings take place near the point of emission, while the photon frequency is still close to line-center. On average, the net radial momentum transfer per emitted photon will likely be dominated by the last scattering event before the photon escapes from the H II region, or by the dust absorption event if it does not. At a given point in the nebula, the incident photons involved in these final events will be only moderately anisotropic. Since there is less than one Ly- $\alpha$  photon created per case B recombination, the total radial momentum deposited by these final events will be a small fraction of the radial momentum of the original ionizing photons. Henney & Arthur (1998) estimate that dust limits the Ly- $\alpha$  radiation pressure to  $\sim 6\%$  of the gas pressure. We conclude that Ly- $\alpha$  has only a minor effect on the density profile within the ionized zone.

## 5.5. H II Region Expansion

H II regions arise when massive stars begin to emit ionizing radiation. The development of the H II region over time depends on the growth of the ionizing output from the central star, and the expansion of the initially-high pressure ionizing gas. Many authors (e.g., Kahn 1954; Spitzer 1978) have discussed the development of an H II region in gas that is initially neutral and uniform. If the ionizing output from the star turns on suddenly, the ionization front is initially “strong R-type”, propagating supersonically without affecting the density of the gas, slowing until it becomes “R-critical”, at which point it makes a transition to “D-type”, with the ionization front now preceded by a shock wave producing a dense (expanding) shell of neutral gas bounding the ionized region.

While the front is R-type, the gas density and pressure are essentially uniform within the ionized zone. When the front becomes D-type, a rarefaction wave propagates inward from the ionization front, but the gas pressure (if radiation pressure effects are not important) remains relatively uniform within the ionized region, because the motions in the ionized gas are subsonic.

When radiation pressure effects are included, the instantaneous density profile interior to the ionization front is expected to be similar to the profile calculated for the static equilibria studied here. Let  $V_i$  be the velocity of the ionization front relative to the star. When the ionization front is weak D-type, the velocity of the ionization front relative to the ionized gas just inside the ionization front is  $\sim 0.5V_i$  (Spitzer 1978). Given the small dust drift velocities  $v_{d,r}$  near the ionization front (i.e.,  $\tau(r) \rightarrow \tau(R)$  in Fig. 7), dust is unable to drift outward across the ionization front as long as the ionization front is propagating outward at  $V_i \gtrsim 0.1 \text{ km s}^{-1}$ .

## 6. Summary

1. Dusty H II regions in static equilibrium consist of a three-parameter family of similarity solutions, parametrized by parameters  $\beta$ ,  $\gamma$ , and a third parameter, which can be taken to be  $Q_{0,49}n_{\text{rms}}$  or  $\tau_{d0}$  (see eq. 14). The  $\beta$  parameter (eq. 6) characterizes the relative importance of  $h\nu < 13.6 \text{ eV}$  photons, and  $\gamma$  (eq. 7) characterizes the dust opacity. A fourth parameter – e.g., the value of  $n_{\text{rms}}$  or  $Q_{0,49}$  – determines the overall size and density of the H II region.
2. Radiation pressure acting on both gas and dust can strongly affect the structure of H II regions. For dust characteristic of the diffuse ISM of the Milky Way, static H II regions with  $Q_{0,49}n_{\text{rms}} \lesssim 10^2 \text{ cm}^{-3}$  will have nearly uniform density, but when  $Q_{0,49}n_{\text{rms}} \gg 10^2 \text{ cm}^{-3}$ , radiation pressure acts to concentrate the gas in a spherical shell.
3. For given  $\beta$  and  $\gamma$ , the importance of radiation pressure is determined mainly by the parameter  $\tau_{d0}$  (see eq. 14). When  $\tau_{d0} \gtrsim 1$ , radiation pressure will produce a noticeable central cavity.
4. For  $\tau_{d0} \gtrsim 1$ , compression of the gas and dust into an ionized shell leads to a substantial increase in the fraction  $f_{\text{ion}}$  of  $h\nu > 13.6 \text{ eV}$  photons that actually ionize H, relative to what would have been estimated for a uniform density H II region, as shown in Fig. 5. Eq. (16) allows  $f_{\text{ion}}$  to be estimated for given  $Q_{0,49}n_{\text{rms}}$ ,  $\beta$ , and  $\gamma$ . Galactic H II regions appear to have values of  $f_{\text{ion}}$  consistent with the present results for H II regions with radiation pressure (see Fig. 9).
5. Interstellar bubbles surrounding O stars are the result of the combined effects of radiation pressure and stellar winds. For the N49 bubble, as an example, the observed ring-like free-free emission profile is more strongly peaked than would be expected from radiation pressure alone, implying that a fast stellar wind must be present to help create the low-density central cavity.

6. For static H II regions, dust drift would be important on time scales  $\lesssim 1\text{Myr}$  for  $Q_{0,49}n_{\text{rms}} \gtrsim 10^3\text{cm}^{-3}$ . Real H II regions are not static, and the dust will not drift out of the ionized gas because the ionization front will generally be propagating (relative to the ionized gas just inside the ionization front) faster than the dust drift speed  $\lesssim 1\text{km s}^{-1}$  (see Fig. 7).

I am grateful to Bob Benjamin for helpful discussions, and to R.H. Lupton for making available the SM graphics package. This research made use of NASA's Astrophysics Data System Service, and was supported in part by NASA through JPL contract 1329088.

## REFERENCES

- Arthur, S. J., Kurtz, S. E., Franco, J., & Albarrán, M. Y. 2004, *ApJ*, 608, 282
- Brown, R. L., & Mathews, W. G. 1970, *ApJ*, 160, 939
- Churchwell, E., et al. 2009, *PASP*, 121, 213
- . 2006, *ApJ*, 649, 759
- Draine, B. T. 1995, *Ap&SS*, 233, 111
- Draine, B. T., & Salpeter, E. E. 1979, *ApJ*, 231, 77
- Figer, D. F., et al. 2002, *ApJ*, 581, 258
- Gail, H. P., & Sedlmayr, E. 1979, *A&A*, 77, 165
- Helfand, D. J., Becker, R. H., White, R. L., Fallon, A., & Tuttle, S. 2006, *AJ*, 131, 2525
- Henney, W. J., & Arthur, S. J. 1998, *AJ*, 116, 322
- Inoue, A. K. 2002, *ApJ*, 570, 688
- Kahn, F. D. 1954, *Bull. Astron. Inst. Netherlands*, 12, 187
- Krumholz, M. R., & Matzner, C. D. 2009, *ApJ*, 703, 1352
- Martins, F., Schaerer, D., & Hillier, D. J. 2005, *A&A*, 436, 1049
- Mathews, W. G. 1967, *ApJ*, 147, 965
- . 1969, *ApJ*, 157, 583
- Petrosian, V., Silk, J., & Field, G. B. 1972, *ApJ*, 177, L69
- Savedoff, M. P., & Greene, J. 1955, *ApJ*, 122, 477

- Spitzer, L. 1968, *Diffuse matter in space* (New York: Interscience)
- . 1978, *Physical Processes in the Interstellar Medium* (New York: Wiley)
- Strömgren, B. 1939, *ApJ*, 89, 526
- Watson, C., et al. 2008, *ApJ*, 681, 1341
- Weingartner, J. C., & Draine, B. T. 2001, *ApJ*, 548, 296
- Zubko, V., Dwek, E., & Arendt, R. G. 2004, *ApJS*, 152, 211